Structure and Bonding in B_6^- and B_6: Planarity and Antiaromaticity

Anastassia N. Alexandrova and Alexander I. Boldyrev*,†

Department of Chemistry and Biochemistry, Utah State University, Logan, Utah 84322-0300

Hua-Jin Zhai and Lai-Sheng Wang*,‡

Department of Physics, Washington State University, 2710 University Drive, Richland, Washington 99352, and W. R. Wiley Environmental Molecular Sciences Laboratory, Pacific Northwest National Laboratory, MS K8-88, P.O. Box 999, Richland, Washington 99352

Erich Steiner and Patrick W. Fowler*,§

School of Chemistry, University of Exeter, Stocker Road, Exeter EX4 4QD, U.K.

Received: August 30, 2002; In Final Form: October 12, 2002

The electronic structure and chemical bonding of B_6^- and B_6 were investigated using anion photoelectron spectroscopy and ab initio calculation. Vibrationally resolved photoelectron spectra were obtained for B_6^- and were compared to calculations performed at various levels of theory. Extensive searches were carried out for the global minimum of B_6^-, which was found to have a planar D_{2h} structure with a doublet ground state ($^2B_{2g}$). Good agreement was observed between ab initio detachment energies and the experimental spectra, establishing that the ground-state structure of B_6^- is planar, in contrast to the three-dimensional structures for the valence-isoelectronic Al_6^- and Al_6 species. The chemical bonding in B_6^- was interpreted in terms of linear combinations of molecular orbitals of two B_3^- fragments. The antiaromatic nature of chemical bonding was established for B_6^- and B_6^{2-}, based on the analysis of orbital contributions to overall paratropic ring currents.

1. Introduction

The most probable configurations of four or more interacting objects are three-dimensional (3D). Planar two-dimensional (2D) clusters with four or more atoms are considered to be unusual, requiring special explanation. Investigations of these systems can reveal new types of chemical bonding, of which the recent discoveries of pentaatomic tetracoordinated planar carbon[1−6] and all-metal aromaticity[7−10] are good examples. Boron is an element well-known for its diverse and complex range of chemistry[11,12] and variety of allotropic modifications. The structural unit that dominates the allotropes of boron is the B_{12} icosahedron. Other 3D-structures are known, such as the B_6 octahedron and the B_{12} cuboctahedron. Two-dimensional boron networks are found in some metal borides; but 3D-structures are dominant in the rich chemistry of the borohydride.[11,12] Hence it may seem that 3D-structures should be expected for pure boron clusters too, but planar or quasi-planar structures have been proposed for small boron clusters, and supported by ab initio calculations.[13−38] Despite many mass-spectrometry-based experimental studies[14,39−45] on small boron clusters during the past decade, experimental information on their geometrical and electronic structures is limited. Detailed spectroscopic investigations would be desirable for gaining insight into the electronic structure and chemical bonding of these electron-deficient cluster species, as well as in testing the available theoretical calculations.

Our recent work has shown that photodetachment photoelectron spectroscopy (PES) combined with ab initio calculations provides a powerful means for obtaining information about the structure and bonding of novel gaseous clusters.[46] In work on B_5^- and B_5, we established the planar ground-state structures for B_5^- (C_{2v}, $^1A_1$) and B_5 (C_{2v}, $^2B_2$).[47] We also investigated the chemical bonding in B_5^- and compared it to that in Al_5^-. While both B_5^- and Al_5^- have a similar C_{2v} planar structure, their π-bonding orbitals are different. In Al_5^-, a π bonding orbital was previously observed to delocalize over only the three central atoms in the C_{2v} ground-state structure,[48] whereas a similar π orbital ($1b_1$) was found to delocalize over all five atoms in B_5^-. This π bonding in B_5^- makes it more rigid than Al_5^- toward butterfly out-of-plane distortions.

In the current paper, we continue our exploration of the structural and electronic properties and chemical bonding in small boron clusters. We report a combined PES and ab initio study of B_6^- and B_6. On one hand, the B_6 octahedron is a common building block in metal borides and borohydrides as mentioned above, and on the other, the valence-isoelectronic Al_6^- and Al_6 clusters are known from ab initio calculations to possess 3D structures.[49−54] The present study shows that B_6^- is planar. A detailed analysis was carried on the structure and bonding of B_6^- and evidence of antiaromaticity was presented for this odd-electron system.

2. Experimental Method

The experiment was carried out using a magnetic-bottle time-of-flight PES apparatus equipped with a laser vaporization supersonic cluster source.[55,56] The B_6^- anions were produced

* To whom correspondence should be addressed.
† E-mail: boldyrev@cc.usu.edu.
‡ E-mail: ls.wang@pnl.gov.
§ E-mail: PWFowler@ex.ac.uk.

10.1021/jp0268866 CCC: $25.00
Published on Web 02/08/2003

by laser vaporization of a pure boron target in the presence of a helium carrier gas. Various clusters were produced from the cluster source and were analyzed using a time-of-flight mass spectrometer. The B_6^- species were mass-selected and decelerated before being photodetached. Three detachment photon energies were used in the current experiments: 355 nm (3.496 eV), 266 nm (4.661 eV), and 193 nm (6.424 eV). The photoelectron spectra were calibrated using the known spectrum of Rh^-, and the resolution of the apparatus was better than 30 meV for 1 eV electrons. Although it was not difficult to observe mass spectra with a wide size range of B_n^- clusters by laser vaporization, it was rather challenging to obtain high quality PES spectra, primarily due to the low photodetachment cross sections of these light clusters and the difficulty of obtaining cold cluster anions. The key to the current progress was the use of a large waiting-room nozzle, which could cool cluster anions more efficiently.[55−57] The temperature effects were further controlled by tuning the timing of the firing of the vaporization laser relative to the carrier gas, and choosing the later part of the cluster beam for photodetachment.[58−61] These efforts have allowed us to obtain well-resolved PES data for a wide size range of B_n^- clusters at different photodetachment energies. We have reported the result of B_5^- recently,[47] and in the current paper we present the result for B_6^- combined with a detailed ab initio study.

3. Computational Methods

We first optimized geometries of B_6, B_6^-, and B_6^{2-} employing analytical gradients with the polarized split-valence basis sets (6-311+G*)[62−64] with a hybrid method, which includes a mixture of Hartree−Fock exchange with density functional exchange-correlation potentials (B3LYP).[65−67] To test the validity of the one-electron approximation, we optimized geometries and calculated frequencies using the multi-configuration self-consistent field method (CASSCF) with nine active electrons for B_6^- and 8 active electrons for the neutral species as well as eight active molecular orbitals in both cases [CASSCF(9,8)/6-311+G* for B_6^- and CASSCF(8,8)/6-311+G* for B_6]. Vertical electron detachment energies (VDEs) from the lowest-energy structure of B_6^- into the excited triplet states of B_6 were calculated using the coupled-cluster RCCSD(T) method[68−71] and unrestricted outer-valence Green function (UOVGF) method.[72−76]

As shown in section V below, B_6^- was found to have a doublet ground state. Thus, both triplet and singlet excited states of the neutrals can be reached in the photodetachment. We were able to calculate the VDEs only to the triplet excited states using the UOVGF and RCCSD(T) methods, because the electron detachment processes leading to singlet excited states would require multiconfiguration reference wave functions. For the lowest detachment channel the final singlet state is essentially single-configuration and therefore we were able to calculate this VDE using the UOVGF and RCCSD(T) methods and the 6-311+G(2df) basis sets. To evaluate VDEs into other singlet final states we used the equation-of-motion method based on the RCCSD(T) wave function [EOM-RCCSD(T)].[77] The core electrons were kept frozen in treating the electron correlation at the UOVGF, RCCSD(T) and EOM-RCCSD(T) levels of theory. All B3LYP/6-311+G*, CASSCF(8,8)/6-311+G*, CASSCF(9,8)/6-311+G*, RCCSD(T)/6-311+G(2df), and UOVGF/6-311+G(2df) calculations were performed using the Gaussian-98 program.[78] The RCCSD(T)/6-311+G(2df) and EOM-RCCSD(T)/6-311+G(2df) were performed using the Molpro-1999 program.[79] Molecular orbitals were calculated at the RHF/6-311+G* and UHF/6-311+G* levels of theory. All MO pictures were made using the MOLDEN 3.4 program.[80]

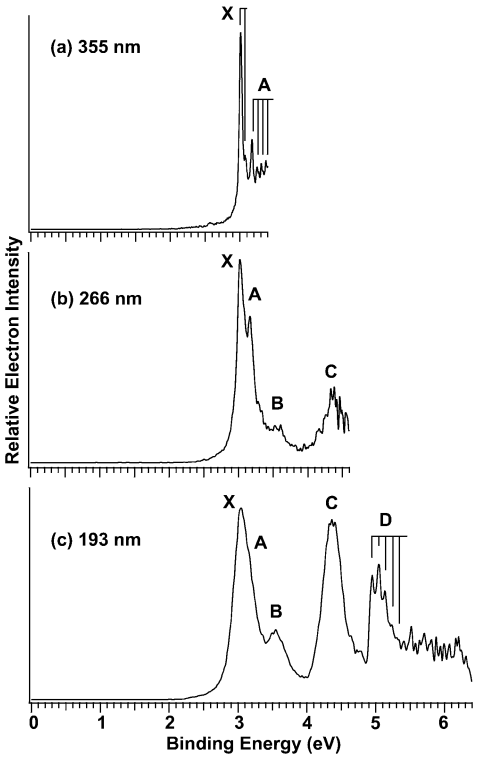

Figure 1. Photoelectron spectra of B_6^- at 355 nm (3.496 eV), 266 nm (4.661 eV), and 193 nm (6.424 eV).

In connection with the discussion of aromaticity/antiaromaticity, maps of the current density induced by a magnetic field directed along the normal to the molecular plane were computed with the ipsocentric[81] coupled-Hartree−Fock CTOCD-DZ method,[82,83] (6-311+G* basis) for the two closed-shell species B_6 and B_6^{2-} held at the optimum geometry of the monoanion (RB3LYP, same basis). The Exeter implementation of the SYSMO program[84] was used. Combination of orbital contributions[81] defined by the ipsocentric method allows deduction of the sense of the ring current in the open-shell species B_6^-.

4. Experimental Results

The photoelectron spectra of B_6^- were recorded at three photon energies, as shown in Figure 1. The observed detachment transitions are labeled with letters, and vertical lines represent the resolved vibrational structures. Five intense and well-resolved bands (X, A, B, C, and D) were observed. Vibrational structures were partially resolved in the bands X and A at 355 nm (Figure 1a) and band D at 193 nm (Figure 1c). Both bands B and C were broad and may contain unresolved electronic transitions. Higher binding energy transitions may exist beyond 5.4 eV, but this part of the spectrum at 193 nm had poor signal-to-noise ratio and was not well resolved.

At 355 nm (Figure 1a), only bands X and A were observed. The ground-state transition (*X*) contained a short vibrational progression with a vibrational spacing of 510 cm^{-1}. Higher vibrational transitions of the X band were apparently overlapped with band A. The adiabatic detachment energy (ADE) of B_6^- was defined by the 0−0 transition of the X band to be 3.01 eV. The 0−0 transition also defined the vertical detachment energy (VDE) of the X band. The tail at the low binding energy side was due to hot band transitions or possibly contributions from minor anion isomers. The band A was relatively weak at 355 nm, but it had a well-defined vibrational progression with a spacing of 530 cm^{-1}, similar to that observed in the X band.

TABLE 1: Observed Adiabatic (ADE) and Vertical (VDE) Detachment Energies of B_6^- and Vibrational Frequencies Observed in the Detachment Transitions[a]

observed feature	ADE (eV)	VDE (eV)	vibrational frequency (cm^{-1})
X	3.01 (0.04)	3.01 (0.04)	510 (40)
A	3.17 (0.04)	3.17 (0.04)	530 (40)
B		3.55 (0.05)	
C	4.13 (0.06)	4.35 (0.05)	
D	4.95 (0.03)	5.04 (0.03)	720 (30)

[a] The values in the parentheses represent the experimental uncertainty.

The A band, representing the first excited state of neutral B_6, has an ADE (and VDE) of 3.17 eV, i.e., an excitation energy of 0.16 eV above the neutral ground state.

At 266 nm (Figure 1b), the intensity of the A band was enhanced. Two weaker and broad bands (B and C) were observed with VDEs at ~3.55 and ~4.35 eV, respectively. The B band was overlapped with the A band, preventing its ADE to be measured, but we were able to estimate the ADE for the C band to be ~4.13 eV. Discernible fine features could be seen in the B and C bands at 266 nm, but no well-defined vibrational progressions were resolved.

At 193 nm (Figure 1c), the X and A bands were no longer resolved. The intensity of the C band was considerably enhanced. In addition, a band D was observed with a surprisingly well resolved vibrational progression. The vibrational spacing of the D band (720 cm^{-1}) was much higher than that observed in the X and A bands. The 0−0 transition of the D band yielded an ADE of 4.95 eV, representing an excitation of 1.94 eV above the neutral B_6 ground state. The VDE of the D band was defined by the 1←0 transition at 5.04 eV.

All the obtained ADEs, VDEs, and vibrational frequencies are given in Table 1.

5. Theoretical Results

We first performed a search for the most stable structures for B_6, B_6^-, and B_6^{2-} using the B3LYP/6-311+G* level of theory. A selected set of the low energy structures identified in the search are presented in Figures 2−4 for the three species, respectively.

Our calculations showed that the most stable B_6^- structure was the planar structure **I** (D_{2h}, $^2B_{2g}$) with a configuration, $1a_g^2 1b_{1u}^2 1b_{2u}^2 2a_g^2 1b_{3g}^2 1b_{3u}^2 3a_g^2 2b_{1u}^2 2b_{2u}^2 1b_{2g}^1$. Slightly higher in energy (by 6.2 kcal/mol at B3LYP/6-311+G*), another planar isomer **II** (C_{2h}, ^2B_u) was found with the electronic configuration, $1a_g^2 1b_u^2 2a_g^2 2b_u^2 3a_g^2 1a_u^2 3b_u^2\ 4a_g^2 1b_g^2\ 4b_u^1$. Other structures were found to be more than 10 kcal/mol higher. The applicability of the one-electron approximation was tested using CASSCF(9,8)/6-311+G* calculations. For the most stable structure **I** we found that even though the Hartree−Fock configuration is still dominant ($C_{HF} = 0.885$), the second configuration ($1a_g^2 1b_{1u}^2 1b_{2u}^2 2a_g^2 1b_{3g}^2 1b_{3u}^2 3a_g^2 2b_{1u}^0 2b_{2u}^2 1b_{2g}^1 4a_g^2$) contributes substantially to the CASSCF wave function ($C_{14} = 0.360$, where the coefficient C_i represents the contribution of the ith excited configuration). We also optimized the geometry for the structure originated from the B_6 pentagonal pyramidal structure C_{5v} ($^1A_1$) by occupying the HOMO with a single electron and allowing it to relax to a local minimum structure **V**, which was found to be 22.7 kcal/mol higher in energy (B3LYP/6-311+G*). Thus, we are confident of the global minimum structure identified for B_6^-. In Table 2, we listed the total energies, structural parameters, and vibrational frequencies of the global minimum structure of B_6^- at B3LYP and CASSCF.

For the neutral B_6 we found that a triplet planar structure **XIII** (C_{2h}, ^3A_u) with an electronic configuration, $1a_g^2 1b_u^2 2a_g^2 2b_u^2 3a_g^2 1a_u^2 3b_u^2 4a_g^2 4b_u^1 1b_g^1$, as the most stable at the B3LYP/6-311+G* level of theory (Figure 3). The triplet **XIV** (D_{2h}, $^3B_{3u}$) structure was found to be a first-order saddle-point with the imaginary-frequency mode leading toward structure **XIII**. A singlet structure **XVIII** (D_{2h}, $^1A_{1g}$) (Table 2) had two imaginary frequencies and upon geometry optimization without symmetry restrictions it yielded the *trans*-structure **XVI** (C_2, ^1A) or the *cis*-structure **XIX** (C_{2v}, $^1A_1$). The planar structure **XVII** (C_{2h}, ^1A_g) was found to be a transition state between two **XVI** structures. Among other low-lying structures, the pentagonal pyramidal structure **XV** (C_{5v}, $^1A_1$), is only 1.2 kcal/mol higher in energy at the B3LYP/6-311+G* level of theory. Again, we ran CASSCF(8,8)/6-311+G* calculations in order to test the validity of the one-electron approximation. Surprisingly, we found at this level of theory that the high-symmetry triplet structure **XIV** (D_{2h}, $^3B_{3u}$) and the structure **XVII** (C_{2h}, ^1A_g) are both local minima contrary to the B3LYP/6-311+G* results. At this point we are not able to prove definitely the presence of the deviation from the D_{2h} and C_{2h}, symmetry, respectively, for the B_6 neutral cluster, but we will use the B3LYP/6-311+G* results in our discussion. The Hartree−Fock configurations are still dominant for structure **XVII** ($C_{HF} = 0.848$), with a substantial contribution from a second configuration ($C_{14} = 0.408$), and for structure **XIV** ($C_{HF} = 0.913$) at the CASSCF-(8,8)/6-311+G* level of theory. The total energies of the lowest B_6 structures were calculated at our highest CCSD(T)/6-311+G-(2df) level of theory using the B3LYP/6-311+G* geometries.

TABLE 2: Calculated Molecular Properties of the D_{2h} Structure I of B_6^- (Figure 2) and Structure XVIII of B_6 (Figure 3)

B_6^-, D_{2h}, $^2B_{2g}$	B3LYP/6-311+G*	CASSCF(9,8)/6-311+G*	B_6, D_{2h}, ^1A_g	B3LYP/6-311+G*	CASSCF(9,8)/6-311+G*
E_{tot}, au	−148.926468	−147.92236	E_{tot}, au	−148.81388	−147.86077
$R(B_1-B_{3,4})$, Å	1.539	1.557	$R(B_1-B_{3,4})$, Å	1.566	1.592
$R(B_3-B_4)$, Å	1.807	1.805	$R(B_3-B_4)$, Å	1.861	1.855
$R(B_3-B_6)$, Å	1.615	1.611	$R(B_3-B_6)$, Å	1.578	1.570
$\omega_1(a_g)$, cm^{-1}	1343	1346	$\omega_1(a_g)$, cm^{-1}	1354	1335
$\omega_2(a_g)$, cm^{-1}	816	843	$\omega_2(a_g)$, cm^{-1}	818	837
$\omega_3(a_g)$, cm^{-1}	626	691	$\omega_3(a_g)$, cm^{-1}	577	642
$\omega_4(a_u)$, cm^{-1}	298	341	$\omega_4(a_u)$, cm^{-1}	13i	202
$\omega_5(b_{2g})$, cm^{-1}	396	455	$\omega_5(b_{2g})$, cm^{-1}	459	454
$\omega_6(b_{3g})$, cm^{-1}	1074	1007	$\omega_6(b_{3g})$, cm^{-1}	1068	1319
$\omega_7(b_{3g})$, cm^{-1}	229	191	$\omega_7(b_{3g})$, cm^{-1}	234	201
$\omega_8(b_{1u})$, cm^{-1}	1165	1174	$\omega_8(b_{1u})$, cm^{-1}	1057	1198
$\omega_9(b_{1u})$, cm^{-1}	676	720	$\omega_9(b_{1u})$, cm^{-1}	601	644
$\omega_{10}(b_{2u})$, cm^{-1}	1333	1414	$\omega_{10}(b_{2u})$, cm^{-1}	1398	1367
$\omega_{11}(b_{2u})$, cm^{-1}	659	707	$\omega_{11}(b_{2u})$, cm^{-1}	676	676
$\omega_9(b_{3u})$, cm^{-1}	206	250	$\omega_9(b_{3u})$, cm^{-1}	76i	171

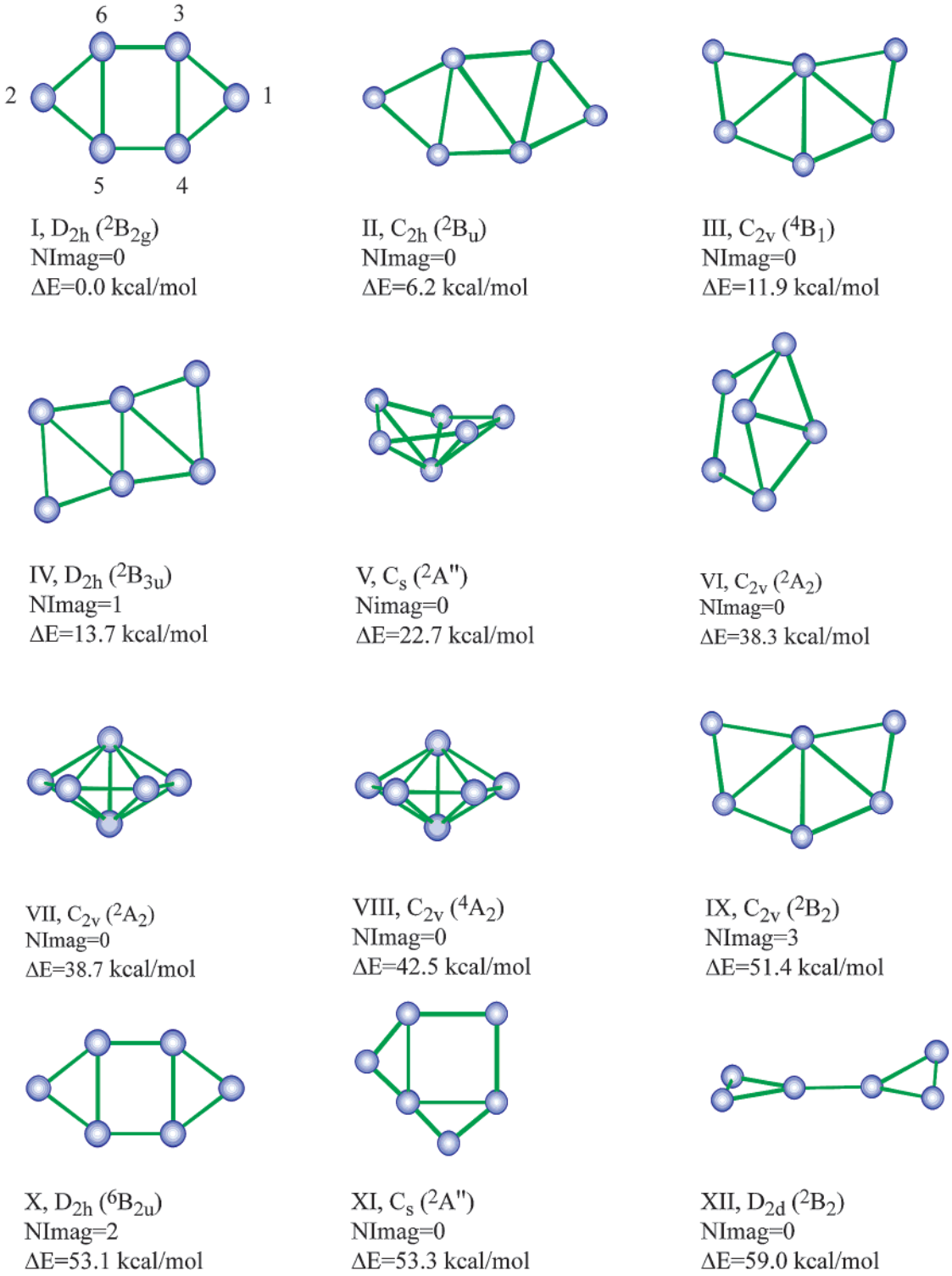

Figure 2. Optimized structures of B_6^- at the B3LYP/6-311+G* level of theory.

We found a different order of the four lowest structures. At this level of theory we found that the pentagonal pyramidal **XV** structure is the most stable, followed by the planar triplet **XIII** structure (7.2 kcal/mol), and then the two singlet **XVI** (8.2 kcal/mol) and **XIX** (9.7 kcal/mol) structures. Total energies, detailed structural parameters, and vibrational frequencies at B3LYP for several isomers of B_6 are given in Table 3.

We also performed a search for the global minimum structure of B_6^{2-}. This dianion is not expected to be stable against autodetachment, but it should have a local minimum as a metastable species.[85,86] Results of our calculations are presented in Figure 4. The structure **XXV** (D_{2h}, ^1A_g) with the configuration, $1a_g^2 1b_{1u}^2 1b_{2u}^2 2a_g^2 1b_{3g}^2 1b_{3u}^2 3a_g^2 2b_{1u}^2\ 2b_{2u}^2 1b_{2g}^2$, was found to be the most stable, consistent with previous results.[87] But this is in contrast to Al_6^{2-}, which was found to be an octahedral global minimum.[88] A similar octahedral structure (**XXXVI**) for B_6^{2-} lies significantly higher in energy.

6. Interpretation of the Photoelectron Spectra and Comparison with Theory

Due to the open shell nature of the B_6^- ground state, photodetachment will yield a set of triplet and singlet final states

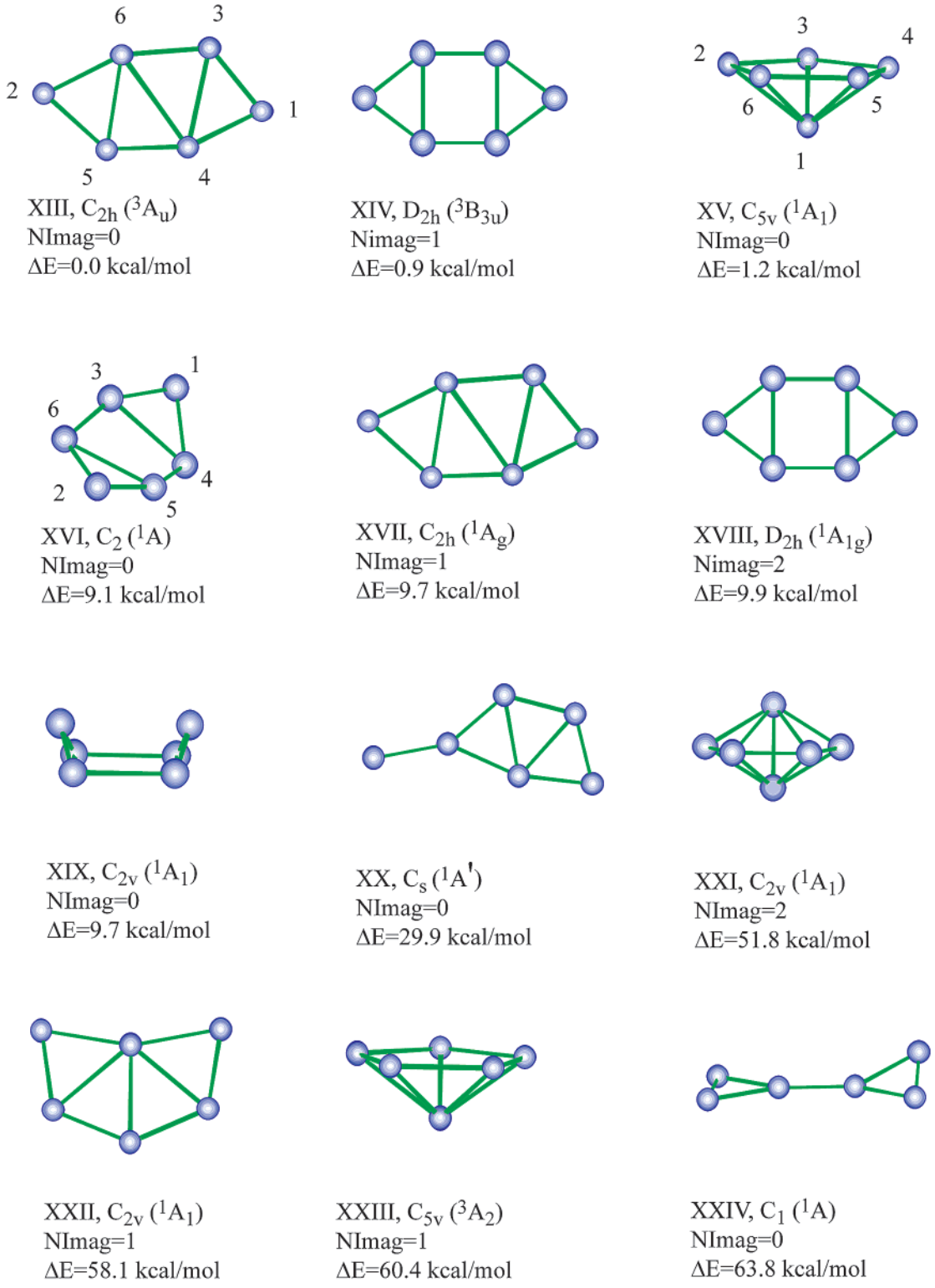

Figure 3. Optimized structures of B_6 at the B3LYP/6-311+G* level of theory.

when removing electrons from doubly occupied MOs of the anion. As mentioned in section III, EOM-RCCSD(T) method had to be used to calculate VDEs for the singlet excited states. In addition, we also found appreciable multi-configurational character of the wave function. Therefore, we will rely primarily on the RCCSD(T)/6-311+G(2df) and RCCSD(T)-EOM/6-311+G(2df) calculations rather than the UOVGF/6-311+G(2df) data (Table 4), when comparing with the experimental results.

6.1. The X and A Bands. The photoelectron spectra of B_6^- showed an intense threshold transition (X), followed by a closely spaced band A. This pattern indicates that the neutral ground-state involved in the detachment transition must also be open shell. If the neutral ground state were closed shell, a weak threshold peak would be expected, followed by a HOMO−LUMO gap and a stronger band. Therefore, the neutral B_6 must have a triplet ground state with a closely spaced singlet state, as revealed by the relatively small separation between the X and A bands (0.16 eV). This experimental observation is directly borne out by our theoretical calculations. Although the C_{5v} structure (**XV**, Figure 3) is a low-lying minimum for neutral

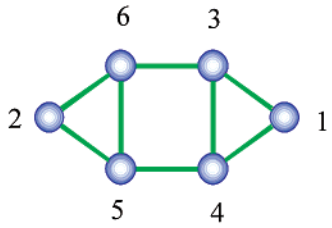

XXV, D_{2h} (^1A_g)
Nimag=0
ΔE=0.0

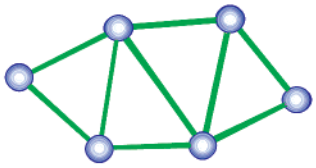

XXVI, C_{2h} (^3B_g)
Nimag=0
ΔE=9.5 kcal/mol

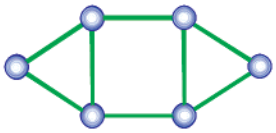

XXVII, D_{2h} ($^3B_{2g}$)
Nimag=1
ΔE=10.9 kcal/mol

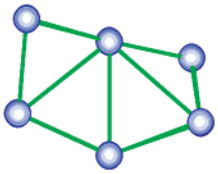

XXVIII, C_2 (^1A)
Nimag=0
ΔE=20.6 kcal/mol

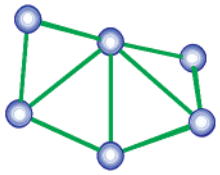

XXIX, C_2 (^3A)
Nimag=1
ΔE=22.2 kcal/mol

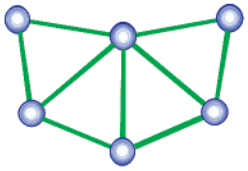

XXX, C_{2v} ($^1A_1$)
NImag=1
ΔE=30.3 kcal/mol

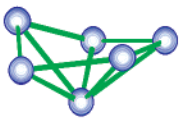

XXXI, C_s ($^1A'$)
Nimag=0
ΔE=36.2 kcal/mol

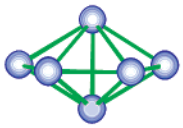

XXXII, C_{2v} ($^1A_1$)
Nimag=1
ΔE=36.3 kcal/mol

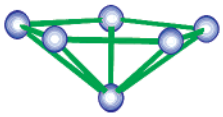

XXXIII, C_{5v} ($^3A_1$)
Nimag=1
ΔE=46.4 kcal/mol

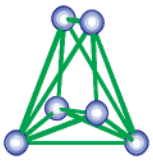

XXXIV, C_{2v} ($^1A_1$)
Nimag=1
ΔE=66.4 kcal/mol

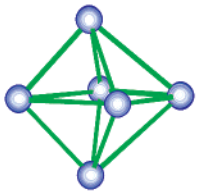

XXXV, D_{2d} ($^1A_1$)
Nimag=0
ΔE=70.8 kcal/mol

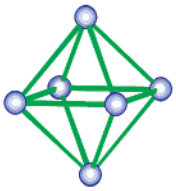

XXXVI, D_{2h} (^1A_g)
Nimag=3
ΔE=71.4 kcal/mol

Figure 4. Optimized structures of B_6^{2-} at the B3LYP/6-311+G* level of theory.

B_6, the closely related anion (**V**, Figure 2) is much higher in energy and would not be observed in the experiment.

The lowest VDE was calculated to be 2.86 eV by detaching a $2b_{2u}$ electron (HOMO-1, Figure 5) to produce the triplet final state $^3B_{3u}$ at the RCCSD(T)/6-311+G(2df) level of theory (Table 4). At the B3LYP/6-311+G* level of theory, the structure **XIV** (D_{2h}, $^3B_{3u}$) was found to be a first-order saddle point and relaxes in the local minimum **XIII** (C_{2h}, ^3A_u). The observed vibrational frequency (510 cm^{-1}) is attributed to the elongation of the B−B distances (B5−B6 and B3−B4 in structure I) upon detachment according to the $2b_{2u}$ orbital. There are five totally symmetric vibrational modes for the C_{2h} B_6 (Table 3). The calculated vibrational frequency for ω_4 (517 cm^{-1}) is in good agreement with the observed vibrational spacing.

TABLE 3: Calculated Molecular Properties of the Structures XIII, XV, and XVI (Figure 3) of B_6

B_6, C_{2h}, ^3A_u	B3LYP/6-311+G*	B_6, C_{5v}, $^1A_1$	B3LYP/6-311+G*	B_6, C_2, ^1A	B3LYP/6-311+G*
E_{tot}, a. u.	−148.82943	E_{tot}, a. u.	−148.82749	E_{tot}, au	−148.81492
$R(B_1-B_3)$, Å	1.516	$R(B_1-B_2)$, Å	1.659	$R(B_1-B_3)$, Å	1.571
$R(B_3-B_4)$, Å	1.845	$R(B_2-B_3)$, Å	1.610	$R(B_1-B_4)$, Å	1.548
$R(B_4-B_6)$, Å	2.012	$R(B_2-B_4)$, Å	2.604	$R(B_3-B_4)$, Å	1.826
$R(B_3-B_6)$, Å	1.583	$\angle(B_2-B_1-B_4)$	103.4	$R(B_3-B_6)$, Å	1.580
$R(B_1-B_4)$, Å	1.579	$\angle(B_2-B_1-B_3)$	58.0	$\angle(B_1-B_4-B_5-B_2)$	35.9
$\omega_1(a_g)$, cm^{-1}	1390	$\omega_1(a_1)$, cm^{-1}	1047	$\omega_1(a)$, cm^{-1}	1292
$\omega_2(a_g)$, cm^{-1}	1081	$\omega_1(a_1)$, cm^{-1}	649	$\omega_2(a)$, cm^{-1}	1072
$\omega_3(a_g)$, cm^{-1}	807	$\omega_1(e_1)$, cm^{-1}	1079	$\omega_3(a)$, cm^{-1}	838
$\omega_4(a_g)$, cm^{-1}	517	$\omega_1(e_1)$, cm^{-1}	1079	$\omega_4(a)$, cm^{-1}	556
$\omega_5(a_g)$, cm^{-1}	264	$\omega_1(e_1)$, cm^{-1}	814	$\omega_5(a)$, cm^{-1}	316
$\omega_6(b_g)$, cm^{-1}	321	$\omega_1(e_1)$, cm^{-1}	814	$\omega_6(a)$, cm^{-1}	203
$\omega_7(b_u)$, cm^{-1}	1329	$\omega_1(e_2)$, cm^{-1}	1112	$\omega_7(a)$, cm^{-1}	171
$\omega_8(b_u)$, cm^{-1}	661	$\omega_1(e_2)$, cm^{-1}	1112	$\omega_8(b)$, cm^{-1}	1349
$\omega_9(b_u)$, cm^{-1}	516	$\omega_1(e_2)$, cm^{-1}	591	$\omega_9(b)$, cm^{-1}	1098
$\omega_{10}(a_u)$, cm^{-1}	332	$\omega_1(e_2)$, cm^{-1}	591	$\omega_{10}(b)$, cm^{-1}	708
$\omega_{11}(a_u)$, cm^{-1}	238	$\omega_1(e_2)$, cm^{-1}	336	$\omega_{11}(b)$, cm^{-1}	567
		$\omega_1(e_2)$, cm^{-1}	336	$\omega_{12}(b)$, cm^{-1}	411

TABLE 4: Theoretical Vertical Detachment Energies (VDE) in eV for B_6^-

	VDE (theor.)		
final state	UOVGF/6-311+G(2df)[a]	RCCSD(T)/6-311+G(2df)	EOM-RCCSD(T)/6-311+G(2df)
$^3B_{3u}$ $(1b_{3u}^2 3a_g^2 2b_{1u}^2 2b_{2u}^1 1b_{2g}^1)$	3.19 (0.86)	2.86	
^1A_g $(1b_{3u}^2 3a_g^2 2b_{1u}^2 2b_{2u}^2 1b_{2g}^0)$	3.05 (0.89)	2.90	
$^1B_{3u}$ $(1b_{3u}^2 3a_g^2 2b_{1u}^2 2b_{2u}^1 1b_{2g}^1)$			3.30
^3A_u $(1b_{3u}^2 3a_g^2 2b_{1u}^1 2b_{2u}^2 1b_{2g}^1)$	4.90 (0.81)	4.06	
^1A_u $(1b_{3u}^2 3a_g^2 2b_{1u}^1 2b_{2u}^2 1b_{2g}^1)$			4.58
$^3B_{2g}$ $(1b_{3u}^2 3a_g^1 2b_{1u}^2 2b_{2u}^2 1b_{2g}^1)$	4.45 (0.89)	4.26	
$^1B_{2g}$ $(1b_{3u}^2 3a_g^1 2b_{1u}^2 2b_{2u}^2 1b_{2g}^1)$			4.75
$^3B_{1u}$ $(1b_{3u}^1 3a_g^2 2b_{1u}^2 2b_{2u}^2 1b_{2g}^1)$	4.68 (0.90)	4.75	
$^1B_{1u}$ $(1b_{3u}^1 3a_g^2 2b_{1u}^2 2b_{2u}^2 1b_{2g}^1)$			5.82

[a] The values in the parentheses indicate the pole strength, which characterizes the validity of the one-electron detachment picture in UOVGF.

The next detachment channel is from the $1b_{2g}$-HOMO of B_6^- (Figure 5) with a calculated VDE of 2.90 eV at the RCCSD-(T)/6-311+G(2df) level of theory and 3.05 eV at the UOVGF/6-311+G(2df) level of theory (Table 4). The RCCSD(T)/6-311+G(2df) VDE is in a good agreement with the measured VDE of 3.01 eV for the A feature. The final state of this detachment channel should correspond to structure **XVI**, relaxed from structure **XVIII** (Figure 3). The observed vibrational frequency (530 cm^{-1}) is in good agreement with that of ω_4(a) (556 cm^{-1}) of the structure **XVI** (Table 3). Overall, the RCCSD-(T)/6-311+G(2df) results appeared to give the right ordering for the X and A bands. The observed discrepancies were not unexpected considering the complexity of the system.

6.2. The B Band. As mentioned above, photodetachment from each doubly occupied MO of B_6^- will yield both a triplet and a singlet final state; the splittings can be large, as expected from the strong electron correlation effects. VDEs for transitions to four low-lying excited singlet final states were calculated at the EOM-RCCSD/6-311+G(2df) level of theory and were given in Table 4. The VDE to the lowest-lying excited singlet final state ($^1B_{3u}$), due to detachment of the spin-up electron from the $2b_{2u}$ orbital of B_6^-, was calculated to be 3.30 eV, which was in good agreement with that of feature B (VDE: 3.55 eV). Therefore, feature B is assigned straightforwardly to the $^1B_{3u}$ final state. We note that the intensity of feature B is much lower than that of feature X, as expected for a transition to a singlet final state relative to a triplet final state. The calculated triplet−singlet splitting of ∼0.44 eV is in excellent agreement with the experimental value (0.54 eV), as measured from the VDE difference of bands X and B (Table 1).

6.3. The C Band. The band C is very broad with discernible signals from ∼4.1 to 4.8 eV, which may contain multiple detachment transitions. The next detachment channel according to the RCCSD(T)/6-311+G(2df) calculation is the removal of an electron from the $2b_{1u}$ MO (Figure 5) with a VDE of 4.06 eV. A large discrepancy in the VDE was observed for this detachment channel between UOVGF and RCCSD(T), owing to the multi-configurational nature of this transition. Hence, the VDE of 4.06 eV from RCCSD(T)/6-311+G(2df) is more reliable, and it is close to the VDE of band C, which should have a major contribution from this transition. The VDE of the accompanying transition to the singlet final state ^1A_u was calculated to be 4.58 eV at RCCSD(T)-EOM/6-311+G(2df) (Table 4). This gives a triplet−singlet splitting of 0.52 eV, very similar to the triplet−singlet splitting calculated from detachment of the $2b_{2u}$ MO. We suspect that the ^1A_u channel was also contained in the broad C band.

The next major detachment channel is from the $3a_g$ orbital. The calculated VDEs for the triplet and singlet final states are 4.26 and 4.75 eV (Table 4) at the RCCSD(T)/6-311+G(2df) and RCCSD(T)-EOM/6-311+G(2df) levels of theory, respectively. These VDEs were within the width of the C band. Thus detachment from the $3a_g$ MO should also contribute to the C band.

6.4. The D Band. The D band was most interesting and a simple vibrational progression was observed unexpectedly with a rather large spacing, suggesting that a high frequency totally symmetric mode was active in the detachment process. The next detachment channel to a triplet final state ($^3B_{1u}$) at a calculated VDE of 4.75 eV (Table 4) was in reasonable agreement with the experimental VDE of 5.04 eV. This channel involved photodetachment from the $1b_{3u}$-HOMO-4, which is a delocalized π orbital. It is expected that detachment from this MO would activate the totally symmetric breathing mode with a high frequency, in excellent agreement with the observed simple vibrational progression and the relatively large vibrational

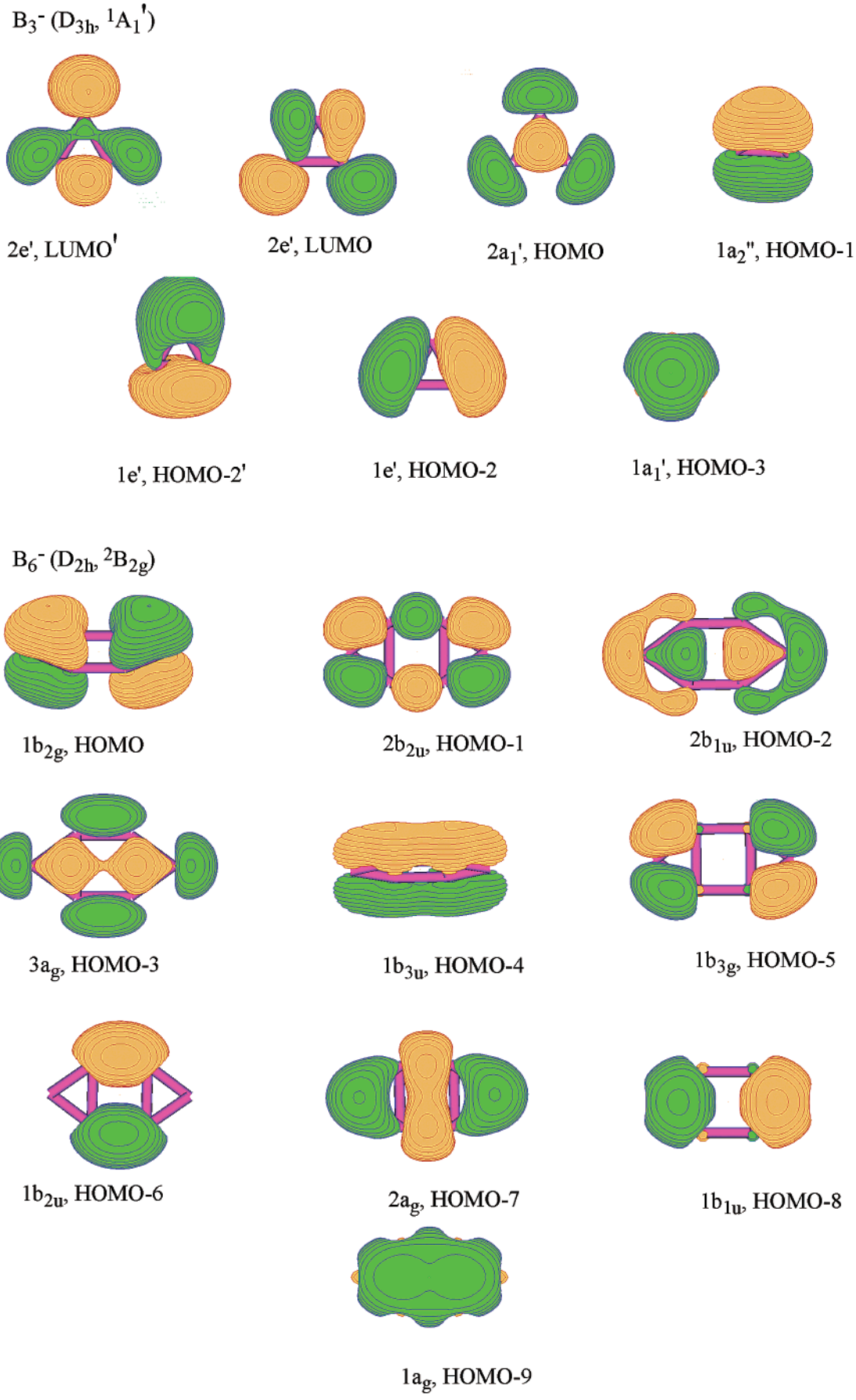

Figure 5. Molecular structure and molecular orbitals of B_3^- and B_6^-.

spacing. The singlet final state for this detachment channel was calculated to have a VDE of 5.82 eV, which should contribute to the broad signals observed beyond 5 eV in the 193 nm spectrum (Figure 1c).

Overall the agreement between the theoretical results at the RCCSD(T)/6-311+G(2df) and RCCSD(T)-EOM/6-311+G(2df) levels of theory and the experimental data is reasonable, confirming the planar D_{2h} structure as the global minimum for B_6^-.

7. Chemical Bonding in B_6^- and B_6 and Antiaromaticity

The elongated shape of the D_{2h} B_6^- ground state (structure **I**) can be understood in terms of the interaction of two B_3^- groups.[89] The HOMO ($2a_1'$) of B_3^- is a σ bonding orbital formed from the in-plane 2p atomic orbitals, as shown in Figure 5. Its HOMO-1 ($1a_2''$) is a π bonding orbital formed from the out-of-plane 2p orbitals. The next three MOs of B_3^- are antibonding/nonbonding ($1e'$) and bonding ($1a_1'$) orbitals formed primarily from the filled 2s valence orbitals with rather small 2p contributions. The LUMO in B_3^- is a degenerate pair of σ^* MOs ($2e'$). When all MOs composed of the same atomic orbitals are occupied, the net bonding effect is expected to be close to zero, as is the case for the $1e'$ and $1a_1'$ MOs in B_3^-, which has only one pair each of σ- and π-bonding electrons.

The MOs of B_6^- can be interpreted as combinations of two B_3^- fragments, with subsequent detachment of an electron from the HOMO of B_6^{2-} (Figure 5). B_6^{2-} is seen to be a 4π system, with bonding arising from four σ- and four π-electrons. It is antiaromatic,[87] as discussed below. B_6^- is thus a 3π system similar in geometric structure to B_6^{2-}. How far does it retain the antiaromaticity of the dianionic species?

Open-shell, and in particular, odd-electron species have received little attention in the aromaticity literature,[90−93] and the CHF CTCD-DZ theory used extensively to map ring currents for closed-shell systems[94] has not yet been implemented for open shells. However, the ipsocentric method in the closed-shell case leads to a decomposition of induced current density into additive orbital contributions that are free of occupied-to-occupied mixing.[81] This fact, combined with the specific symmetries of the occupied orbitals in the present case, allows deduction of the ring-current pattern for B_6^- in the approximation that spin and orbital magnetism effects are completely uncoupled.

The electronic configurations of the neutral, monoanion, and dianion of B_6, assuming a frozen geometry appropriate to the singly charged species, differ only in the occupation of the π orbital of b_{2g} symmetry (Figure 5), which is the HOMO of both B_6^- and B_6^{2-} at this geometry. Computed current-density maps for the two closed-shell species are shown in Figure 6. In each case, the total ($\sigma+\pi$), σ-only, and π-only contributions are plotted at a height of 1 bohr above the molecular plane. In the dianion, the total current is a superposition of a paramagnetic π ring current confined to the inner square of B atoms, and a set of σ paramagnetic vortices localized on the B centers. In the neutral species, the $1b_{2g}$ orbital is empty, and the HOMO π current is absent. The total map for B_6 is now essentially identical with its σ-only map, and is little changed from the σ-only map for the dianion. A small diamagnetic π current is also contributed in the neutral by the two remaining π electrons, which occupy the low-lying $1b_{3u}$ orbital.

These observations have a ready interpretation in the ipsocentric model, in terms of the orbital contributions. For a planar system subjected to a perpendicular magnetic field the induced current density can be partitioned rigorously into a sum over orbital excitations,[81] each of which corresponds either to an in-plane translational transition (producing a diamagnetic current) or to an in-plane rotational transition (producing a paramagnetic current). Both types of transition preserve $\sigma-\pi$ separation.

The large π current in the dianion arises from the rotationally allowed (and therefore paratropic) transitions between the

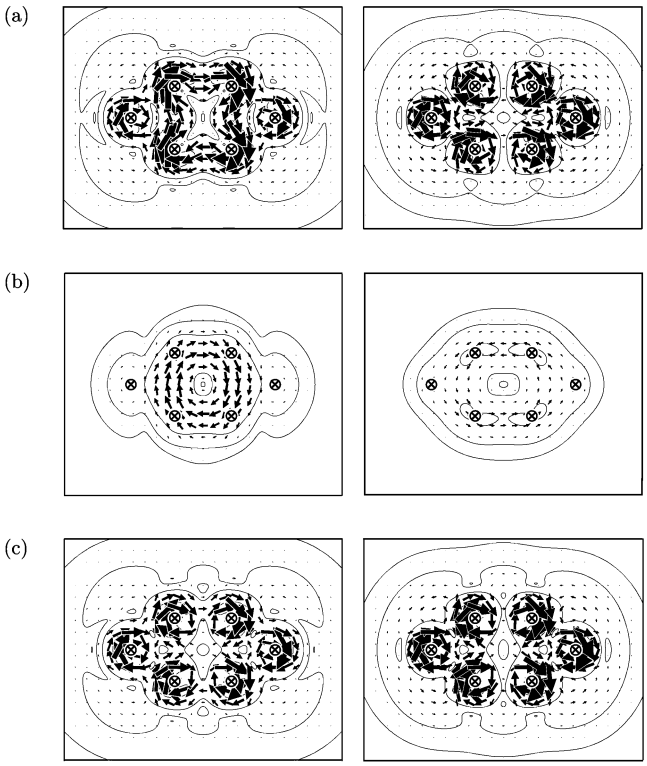

Figure 6. Computed current-density maps at 1 a_0 above the molecular plane for dianionic (left) and neutral (right) D_{2h} hexa-boron rings at the geometry of the monoanion. Diamagnetic circulation is shown anticlockwise, paramagnetic circulation clockwise. Arrows indicate the projection of the current density vector in the plotting plane. (a) All-electron ($\sigma+\pi$) current density, (b) total π current density, and (c) total σ current density.

occupied $1b_{2g}$ HOMO and the empty $1b_{1g}$ orbital that would form the other half of a $\Lambda = 1$ pair in the ideal six-membered ring.[87] The σ currents result from a combination of contributions from HOMO-1 and lower-lying orbitals, and originate from transitions to virtual orbitals that are related by local rotations.[87,95,96] Likewise, in neutral B_6, the loss of the HOMO π pair removes the main contribution to the π current, leaving the σ current essentially undisturbed, but opening up the new translationally allowed $\pi \rightarrow \pi^*$ channel from which the weak diamagnetic current arises.

In open-shell systems, the allowed translational and rotational transitions describing the first-order response of the orbital current density to the external field are between spin−orbitals with the same component of spin. The ipsocentric model for the monoanion therefore predicts that this species will have essentially the same σ current as in B_6 and B_6^{2-}, plus a significant HOMO π current of the same kind as in B_6^{2-}, but with reduction in intensity as only 1 π electron is now participating, plus a small diamagnetic b_{3u} π current as in B_6, again reduced as only one 'hole' is available in the b_{2g} SOMO. Hence, B_6^- is predicted to have a paramagnetic ring current dominated by its least-bound π electron, and therefore to be antiaromatic on the magnetic criterion.

It may be mentioned that calculations of the same kind on B_3^-, the formal precursor of B_6^-, show that this two π-electron system supports a diamagnetic ring current, but these calculations also show that the current is dominated by the strong in-plane σ contribution of the four electrons of the HOMO-2 orbitals, and has only a weak contribution from the two π electrons of the HOMO. Hence B_3^- is aromatic on the magnetic criterion,[97] but, like Al_4^{2-},[98] is more σ- rather than π-aromatic.

The concept of aromaticity in deltahedral boranes was already advanced by Aihara[99] and by King and Rouvray[100] and reviewed recently by King.[101] In the current work we have explored the aromaticity/antiaromaticity concept in pure boron clusters. It may be hoped that the aromaticity concept will be as useful in inorganic chemistry as it is in organic chemistry.

8. Conclusions

The electronic structure and chemical bonding of B_6^- and B_6 were investigated using anion photoelectron spectroscopy and ab initio calculations. Vibrationally resolved photoelectron spectra were obtained for B_6^- and were compared to theoretical calculations performed at various levels of theory. Extensive searches were carried out for the global minimum of B_6^-, which was found to be a planar D_{2h} structure with a doublet ground state ($^2A_{2g}$). Good agreement was observed between ab initio detachment energies and the experimental spectra, establishing that the ground-state structure of B_6^- is planar, in contrast to the 3D structure found for the isoelectronic Al_6^- species. The chemical bonding in B_6^- can be interpreted in terms of combinations of two B_3^- fragments. The antiaromatic nature of B_6^- is established by orbital analysis of ring current effects in the series B_6, B_6^-, and B_6^{2-} at the D_{2h} equilibrium geometry of the monoanion.

Acknowledgment. The theoretical work done at Utah was supported by the donors of the Petroleum Research Fund (ACS-PRF Grant 38242-AC6), administered by the American Chemical Society. The experimental work done at Washington was supported by the National Science Foundation (DMR-0095828) and performed at the W. R. Wiley Environmental Molecular Sciences Laboratory, a national scientific user facility sponsored by DOE's Office of Biological and Environmental Research and located at Pacific Northwest National Laboratory, which is operated for DOE by Battelle.

References and Notes

(1) Li, X.; Wang, L. S.; Boldyrev, A. I.; Simons, J. *J. Am. Chem. Soc.* **1999**, *121*, 6033.
(2) Wang, L. S.; Boldyrev, A. I.; Li, X.; Simons, J. *J. Am. Chem. Soc.* **2000**, *122*, 7681.
(3) Boldyrev, A. I.; Simons, J.; Li, X.; Wang, L. S. *J. Chem. Phys.* **1999**, *111*, 4993.
(4) Li, X.; Zhang, H. F.; Wang, L. S.; Geske, G. D.; Boldyrev, A. I. *Angew. Chem., Int. Ed.* **2000**, *39*, 3630.
(5) Boldyrev, A. I.; Li, X.; Wang, L. S. *Angew. Chem., Int. Ed.* **2000**, *39*, 3307.
(6) Li, X.; Zhai, H. J.; Wang, L. S. *Chem. Phys. Lett.* **2002**, *357*, 415.
(7) Li, X.; Kuznetsov, A. E.; Zhang, H. F.; Boldyrev, A. I.; Wang, L. S. *Science* **2001**, *291*, 959.
(8) Li, X.; Zhang, H. F.; Wang, L. S.; Kuznetsov, A. E.; Cannon, N. A.; Boldyrev, A. I. *Angew. Chem., Int. Ed.*, **2001**, 40, 1867.
(9) Kuznetsov, A. E.; Wang, L. S.; Corbett, J. D.; Boldyrev, A. I. *Angew. Chem., Int. Ed.* **2001**, *40*, 3369.
(10) Boldyrev, A. I.; Kuznetsov, A. E. *Inorg. Chem.* **2002**, *41*, 532.
(11) Cotton, F. A.; Wilkinson, G.; Murillo, C. A.; Bochmann, M. *Advanced Inorganic Chemistry*, 6th ed.; John Wiley & Sons: New York, 1999.
(12) Greenwood, N. N.; Earnshaw, A. *Chemistry of the Elements*, 2nd ed.; Butterworth-Heinemann: Oxford, U. K., 1997.
(13) Tang, A. C.; Li, Q. S. *Int. J. Quantum Chem.* **1986**, *29*, 579.
(14) Hanley, L.; Whitten, J. L.; Anderson, S. L. *J. Phys. Chem.* **1988**, *92*, 5803.
(15) Hernandez, R.; Simons, J. *J. Chem. Phys.* **1991**, *94*, 2961.
(16) Kato, A. U.; Tanaka, E. *J. Comput. Chem.* **1991**, *12*, 1097.
(17) Kato, A. U.; Yamashita, K.; Morokuma, K. *Chem. Phys. Lett.* **1992**, *190*, 361.
(18) Martin, J. M. L.; Francois, J. P.; Gijbels, R. *Chem. Phys. Lett.* **1992**, *189*, 529.
(19) Kawai, R.; Weare, J. H. *Chem. Phys. Lett.* **1992**, *191*, 311.
(20) Ray, A. K.; Howard, I. A.; Kanal, K. M. *Phys. Rev. B* **1992**, *45*, 14247.
(21) Boustani, I. *Int. J. Quantum Chem.* **1994**, *52*, 1081.
(22) Meden, A.; Mavri, J.; Bele, M.; Pejovnik, S. *J. Phys. Chem.* **1995**, *99*, 4252.
(23) Boustani, I. *Chem. Phys. Lett.* **1995**, *233*, 273.
(24) Boustani, I. *Chem. Phys. Lett.* **1995**, *240*, 135.
(25) Boustani, I. *Surf. Sci.* **1996**, *370*, 355.
(26) Ricca, A.; Bauschlicher, C. W. *Chem. Phys.* **1996**, *208*, 233.
(27) Ricca, A.; Bauschlicher, C. W. *J. Chem. Phys.* **1997**, *106*, 2317.
(28) Niu, J.; Rao, B. K.; Jena, P. *J. Chem. Phys.* **1997**, *107*, 132.
(29) Boustani, I. *Phys. Rev. B* **1997**, *55*, 16426.
(30) Gu, F. L.; Yang, X. M.; Tang, A. C.; Jiao, H. J.; Schleyer, P. v. R. *J. Comput. Chem.* **1998**, *19*, 203.
(31) Boustani, I.; Quandt, A. *Comput. Mater. Sci.* **1998**, *11*, 132.
(32) Boustani, I.; Rubio, A.; Alonso, J. A. *Chem. Phys. Lett.* **1999**, *311*, 21.
(33) McKee, M. L.; Wang, Z. X.; Schleyer, P. v. R. *J. Am. Chem. Soc.* **2000**, *122*, 4781.
(34) Fowler, J. E.; Ugalde, J. M. *J. Phys. Chem. A* **2000**, *104*, 397.
(35) Aihara, J. *J. Phys. Chem. A* **2001**, *105*, 5486.
(36) Cao, P.; Zhao, W.; Li, B.; Song, B.; Zhou, X. *J. Phys.: Condens. Matter* **2001**, *13*, 5065.
(37) Petters, A.; Alsenoy, C. V.; March, N. H.; Klein, D. J.; Van Doren, V. E. *J. Phys. Chem. B* **2001**, *105*, 10546.
(38) Luo, W.; Clancy, P. *J. Appl. Phys.* **2001**, *89*, 1596.
(39) Hanley, L.; Anderson, S. L. *J. Phys. Chem.* **1987**, *91*, 5161.
(40) Hanley, L.; Anderson, S. L. *J. Chem. Phys.* **1988**, *89*, 2848.
(41) Hintz, P. A.; Ruatta, S. A.; Anderson, S. L. *J. Chem. Phys.* **1990**, *92*, 292.
(42) Ruatta, S. A.; Hintz, P. A.; Anderson, S. L. *J. Chem. Phys.* **1991**, *94*, 2833.
(43) Hintz, P. A.; Sowa, M. B.; Ruatta, S. A.; Anderson, S. L. *J. Chem. Phys.* **1991**, *94*, 6446.
(44) Placa, S. J. La; Roland, P. A.; Wynne, J. J. *Chem. Phys. Lett.* **1992**, *190*, 163.
(45) Sowa-Resat, M. B.; Smolanoff, J.; Lapiki, A.; Anderson, S. L. *J. Chem. Phys.* **1997**, *106*, 9511.
(46) Boldyrev, A. I.; Wang, L. S. *J. Phys. Chem. A* **2001**, *105*, 10759.
(47) Zhai, H. J.; Wang, L. S.; Alexandrova, A. N.; Boldyrev, A. I. *J. Chem. Phys.* (in press).
(48) Geske, G. D.; Boldyrev, A. I.; Li, X.; Wang, L. S. *J. Chem. Phys.* **2000**, *113*, 5130.
(49) Upton, T. H. *J. Chem. Phys.* **1987**, *86*, 7054.
(50) Petterson, L. G. M.; Bauschlicher, C. W.; Halicioglu, T., Jr. *J. Chem. Phys.* **1987**, *87*, 2205.
(51) Jug, K.; Schluff, H. P.; Kupka, H.; Iffert, R. *J. Comput. Chem.* **1988**, *9*, 803.
(52) Jones, R. O. *J. Chem. Phys.* **1993**, *99*, 1194.
(53) Ahlrichs, R.; Elliott, S. D. *Phys. Chem. Chem. Phys.* **1999**, *1*, 13.
(54) Rao, B. K.; Jena, P. *J. Chem. Phys.* **1999**, *111*, 1890.
(55) Wang, L. S.; Cheng, H. S.; Fan, J. *J. Chem. Phys.* **1995**, *102*, 9480.
(56) Wang, L. S.; Wu, H. in *Advances in Metal and Semiconductor Clusters. IV. Cluster Materials*; Duncan, M. A.; JAI Press: Greenwich, 1998; p 299.
(57) Wang, L. S.; Conceicao, J.; Jin, C.; Smalley, R. E. *Chem. Phys. Lett.* **1991**, *182*, 5.
(58) Wang, L. S.; Li, X. in *Clusters and Nanostructure Interfaces*; Jena P., Khanna, S. N., Rao, B. K., Eds.; World Scientific: New Jersey, 2000; p 293.
(59) Li, X.; Wu, H.; Wang, X. B.; Wang, L. S. *Phys. Rev. Lett.* **1998**, *81*, 1909.
(60) Akola, J.; Manninen, M.; Hakkinen, H.; Landman, U.; Li, X.; Wang, L. S. *Phys. Rev. B* **1999**, *60*, 11297.
(61) Liu, S. R.; Zhai, H. J.; Wang, L. S. *Phys. Rev. B* **2001**, *64*, 153402.
(62) McLean, A. D.; Chandler, G. S. *J. Chem. Phys.* **1980**, *72*, 5639.
(63) Clark, T.; Chandrasekhar, J.; Spitznagel, G. W.; Schleyer, P. v. R. *J. Comput. Chem.* **1983**, *4*, 294.
(64) Frisch, M. J.; Pople, J. A.; Binkley, J. S. *J. Chem. Phys.* **1984**, *80*, 3265.
(65) Parr, R. G.; Yang, W. *Density-Functional Theory of Atoms and Molecules*; Oxford University Press: Oxford, U.K., 1989.
(66) Becke, A. D. *J. Chem. Phys.* **1993**, *98*, 5648.
(67) Perdew, J. P.; Chevary, J. A.; Vosko, S. H.; Jackson, K. A.; Pederson, M. R.; Singh, D. J.; Fiolhais, C. *Phys. Rev. B* **1992**, *46*, 6671.
(68) Krishnan, R.; Binkley, J. S.; Seeger, R.; Pople, J. A. *J. Chem. Phys.* **1980**, *72*, 650.
(69) Cizek, J. *Adv. Chem. Phys.* **1969**, *14*, 35.
(70) Knowles, P. J.; Hampel, C.; Werner, H.-J. *J. Chem. Phys.* **1993**, *99*, 5219.
(71) Raghavachari, K.; Trucks, G. W.; Pople, J. A.; Head-Gordon, M. *Chem. Phys. Lett.* **1989**, *157*, 479.
(72) Cederbaum, L. S. *J. Phys B* **1975**, *8*, 290.
(73) von Niessen, W.; Shirmer, J.; Cederbaum, L. S. *Comput. Phys. Rep.* **1984**, *1*, 57.

(74) Zakrzewski, V. G.; von Niessen, W. *J. Comput. Chem.* **1993**, *14*, 13.

(75) Zakrzewski, V. G.; Ortiz, J. V. *Int. J. Quantum Chem.* **1995**, *53*, 583.

(76) For a recent review, see: Ortiz, J. V.; Zakrzewski, V. G.; Dolgunitcheva, O. *Concept. Trends Quantum Chem.* **1997**, *3*, 463.

(77) Stanton, J. F.; Bartlett, R. J. *J. Chem. Phys.* **1993**, *99*, 7029 and references therein.

(78) Frisch, M. J.; Trucks, G. W.; Schlegel, H. B.; Scuseria, G. E.; Robb, M. A.; Cheeseman, J. R.; Zakrzewski, V. G.; Montgomery, J. A., Jr.; Stratmann, R. E.; Burant, J. C.; Dapprich, S.; Millam, J. M.; Daniels, A. D.; Kudin, K. N.; Strain, M. C.; Farkas, O.; Tomasi, J.; Barone, V.; Cossi, M.; Cammi, R.; Mennucci, B.; Pomelli, C.; Adamo, C.; Clifford, S.; Ochterski, J.; Petersson, G. A.; Ayala, P. Y.; Cui, Q.; Morokuma, K.; Malick, D. K.; Rabuck, A. D.; Raghavachari, K.; Foresman, J. B.; Cioslowski, J.; Ortiz, J. V.; Stefanov, B. B.; Liu, G.; Liashenko, A.; Piskorz, P.; Komaromi, I.; Gomperts, R.; Martin, R. L.; Fox, D. J.; Keith, T.; Al-Laham, M. A.; Peng, C. Y.; Nanayakkara, A.; Gonzalez, C.; Challacombe, M.; Gill, P. M. W.; Johnson, B. G.; Chen, W.; Wong, M. W.; Andres, J. L.; Head-Gordon, M.; Replogle, E. S.; Pople, J. A. *Gaussian 98*, revision A.7; Gaussian, Inc.: Pittsburgh, PA, 1998.

(79) Werner, H.-J.; Knowles, P. J.; with contributions from Amos, R. D.; Bernhardsson A.; Berning A.; Celani P.; Cooper D. L.; Deegan M. J. O.; Dobbyn A. J.; Eckert F.; Hampel C.; Hetzer G.; Korona T.; Lindh R.; Llpyd A. W.; McNicholas S. J.; Manby F. R.; Meyer W.; Mura M. E.; Nicklass A.; Palmieri P.; Pitzer R.; Rauhut G.; Schutz M.; Stoll H.; Stone A. J.; Tarroni R.; Thorsteinsson T. *MOLPRO-1999*.

(80) MO pictures were made using the MOLDEN3.4 program. Schaftenaar, G. *MOLDEN3.4*; CAOS/CAMM Center: The Netherlands, 1998.

(81) Steiner, E.; Fowler, P. W. *J. Phys. Chem. A* **2001**, *105*, 9553.

(82) Keith, T. A.; Bader, R. F. W. *Chem. Phys. Lett.* **1993**, *210*, 223.

(83) Coriani, S.; Lazzeretti, P.; Malagoli, M.; Zanasi, R. **1994**, *89*, 181.

(84) Lazzeretti, P.; Zanasi, R. *SYSMO* package (University of Modena), 1980, with additional routines for evaluation and plotting of current density by E. Steiner, P. W. Fowler (University of Exeter, UK).

(85) Wang, X. B.; Wang, L. S. *Nature* **1999**, *400*, 245.

(86) Ding, C. F.; Wang, X. B.; Wang, L. S. *J. Phys. Chem. A* **1998**, *102*, 8633.

(87) Havenith, R. W. A.; Fowler, P. W.; Steiner, E. *Chem. Eur. J.* **2002**, *8*, 1068.

(88) Kuznetsov, A. E.; Boldyrev, A. I.; Zhai, H. J.; Li, X.; Wang, L. S. *J. Am. Chem. Soc.* **2002**, *124*, 11791.

(89) Kuznetsov, A. E.; Boldyrev, A. I. *Struct. Chem.* **2002**, *13*, 141.

(90) Baird, N. C., *J. Am. Chem. Soc.* **1972**, *94*, 4941.

(91) Gogonea, V.; Schleyer, P. v. R.; Schreiner, P. R. *Angew. Chem., Int. Ed.* **1998**, *37*, 1945.

(92) Minkin, V. I.; Glukhovtsev, M. N.; Simkin, B. Y. *Aromaticity and Antiaromaticity. Electronic and Structural Aspects*; J. Wiley & Sons: New York, 1994.

(93) Kuznetsov, A. E.; Zhai, H. J.; Li, X.; Wang, L. S.; Boldyrev, A. I. *Inorg. Chem.* **2002**, *41*, 6062.

(94) Steiner, E.; Fowler, P. W. *Int. J. Quantum Chem.* **1996**, *60*, 609. Cadioli, B.; Fowler, P. W.; Steiner, E.; Zanasi, R., *J. Phys. Chem. A* **1998**, *102*, 7297; Steiner, E.; Fowler, P. W.; Jenneskens, L. W. *Angew. Chem., Int. Ed.* **2001**, *40* 362. Havenith, R. W. A.; Fowler, P. W.; Steiner, E. *J. Chem. Soc., Perkin Trans.* **2002**, *2*, 502. Steiner, E.; Fowler, P. W.; Havenith, R. W., *J. Phys. Chem. A* **2002**, *106*, 7048.

(95) Fowler, P. W.; Steiner, E. *J. Phys. Chem. A* **2001**, *105*, 9553.

(96) Steiner, E.; Fowler, P. W.; Havenith, R. W. *J. Phys. Chem. A* **2002**, *106*, 7048.

(97) Fowler, P. W.; Steiner, E. Unpublished results.

(98) Fowler, P. W.; Havenith, R. W. A.; Steiner, E. *Chem. Phys. Lett.* **2001**, *342*, 85. Steiner, E.; Fowler, P. W.; Havenith, R. W. *Chem. Phys. Lett.* **2002**, *359*, 530.

(99) Aihara, J.-I. *J. Am. Chem. Soc.* **1978**, *100*, 3339; *Inorg. Chem.* **2001**, *40*, 5042.

(100) King, R. B.; Rouvray, D. H. *J. Am. Chem. Soc.* **1977**, *99*, 7834.

(101) King, R. B. *Chem. Rev.* **2001**, *101*, 1119.